Baltic Astronomy, vol. 23, 151–170, 2014

HOW DOES THE MASS TRANSPORT IN DISK GALAXY MODELS INFLUENCE THE CHARACTER OF ORBITS?

Euaggelos E. Zotos

Department of Physics, School of Science, Aristotle University of Thessaloniki, GR-541 24, Thessaloniki, Greece; e-mail: evzotos@physics.auth.gr

Received: 2014 August 29; accepted: 2014 September 18

Abstract. We explore the regular or chaotic nature of orbits of stars moving in the meridional (R, z) plane of an axially symmetric time-dependent disk galaxy model with a central, spherically symmetric nucleus. In particular, mass is linearly transported from the disk to the galactic nucleus, in order to mimic, in a way, the case of self-consistent interactions of an actual N-body simulation. We thus try to unveil the influence of this mass transportation on the different families of orbits of stars by monitoring how the percentage of chaotic orbits, as well as the percentages of orbits of the main regular resonant families, evolve as the galaxy develops a dense and massive nucleus in its core. The SALI method is applied to samples of orbits in order to distinguish safely between ordered and chaotic motion. In addition, a method based on the concept of spectral dynamics is used for identifying the various families of regular orbits and also for recognizing the secondary resonances that bifurcate from them. Our computations strongly suggest that the amount of the observed chaos is substantially increased as the nucleus becomes more massive. Furthermore, extensive numerical calculations indicate that there are orbits which change their nature from regular to chaotic and vice versa and also orbits which maintain their orbital character during the galactic evolution. The present outcomes are compared to earlier related work.

Key words: galaxies: kinematics and dynamics – structure – chaos

1. INTRODUCTION

A convenient way for studying autonomous Hamiltonian systems is by choosing some values of the total orbital energy, for which the position as well as the extent of ordered and chaotic domains are time-independent (TI) and can be accurately determined by a variety of dynamical methods, especially in the case of low degrees of freedom. The dynamical structure however, in such time-independent Hamiltonian systems is usually very complex due to the presence of "weak" and "strong" chaos. In addition, the motion of test particles takes place on invariant tori of multiple dimensions and it can also display surprising localization properties in both configuration and phase space. It is therefore natural to assume that time-dependent (TD) Hamiltonian systems are expected to exhibit a much more

complicated nature since all the above-mentioned attributes evolve with time due to the absence of any kind of integrals of motion (i.e., the total energy integral) which are valid only in TI systems. Indeed, it is true that in TI systems orbits maintain their orbital character: if for example, an orbit is initially regular it will always remain so, while if it is chaotic it might get trapped near the boundaries of stability regions for relatively long time intervals (this phenomenon is known as "sticky motion") but it will certainty never relinquish its chaoticity. On the other hand, in TD Hamiltonians sudden transitions form regularity to chaoticity and vice versa is a common behavior for individual trajectories during their time-evolution.

The determination of ordered and chaotic properties of motion in time-dependent galactic as well as cosmological models constitutes an extended research area in the field on non-linear dynamics. In a previous work, Caranicolas & Papadopoulos (2003) used a simple analytic time-dependent model in order to study the transition from order to chaos in a galaxy, when mass is exponentially transported from the disk to the galactic core thus forming a dense and massive spherical nucleus. They found that during the galactic evolution a large portion of low angular momentum stars change their orbital nature from regular to chaotic. The investigation was continued in more detail in Zotos (2012) where it was proved by conducting a systematic and thorough exploration of the phase space that during the mass transportation stars do not change their character only from regular to chaotic. In fact, there is a considerable amount of stars which maintain their orbital nature, while there is also a small fraction of star orbits that change their character from chaotic to regular. Furthermore, Papadopoulos & Caranicolas (2006) revealed the orbital behavior in a time-dependent double-barred galaxy model when mass is transported from the primary bar to the inner disk reporting that the galactic evolution significantly affects the nature of orbits. The interplay between ordered and chaotic motion in a time-dependent Hamiltonian describing a barred galaxy was examined in Manos et al. (2013), where it was observed that the percentage of chaos increases when a linear mass transportation from the disk to the bar takes place. In the same vein, Manos & Machado (2014) constructed an analytical time-dependent potential, modeling the gravitational potentials of disk, a bar and a dark matter halo, whose time-dependent parameters are derived from a simulation.

Knowing whether the orbits are regular or chaotic is only the first step toward the understanding of the overall behavior of the disk galaxy. The second and beyond any doubt the most interesting step is the distribution of regular orbits into different families. In our study therefore, once the orbits have been characterized as regular or chaotic, we then further classified the regular orbits into different families by using a frequency analysis method (Carpintero & Aguilar 1998; Muzzio et al. 2005). Initially, Binney & Spergel (1982, 1984) proposed a technique, dubbed spectral dynamics, for this particular purpose. Later on, this method has been extended and improved by Šidlichovský & Nesvorný (1996) and Carpintero & Aguilar (1998). In the recent work of Zotos & Carpintero (2013) the algorithm was refined even further so it can be used to classify orbits in the meridional plane. In general terms, this method computes the Fourier transform of the coordinates of an orbit, identifies its peaks, extracts the corresponding frequencies, and searches for the fundamental frequencies and their possible resonances. Thus, we can easily identify the various families of regular orbits and also recognize the

secondary resonances that bifurcate from them. This technique has been successfully applied in several previous papers (e.g., Zotos & Carpintero 2013; Caranicolas & Zotos 2013; Zotos & Caranicolas 2013, 2014; Zotos 2014a,b) in the field of orbit classification (not only regular versus chaotic, but also separating regular orbits into different regular families) in different galactic gravitational potentials.

The motivation of the present work is to apply the time-dependent version of the disk galaxy model used in Zotos & Carpintero (2013) in order to examine the dynamical properties and the time-evolution of orbits as mass is transferred from the disk to the central nucleus. Moreover, this time-dependent Hamiltonian can, in a way, mimic certain realistic aspects that arise in N-body simulations. Our paper is organized as follows: in Section 2, we explain in detail the properties of the time-dependent disk galaxy model, while Section 3 is devoted to the description of the computational methods we used in order to determine the character as well as the classification of the orbits. A thorough numerical analysis regarding the influence of the mass transport to the percentages of the different families of orbits is performed in Section 4. Our paper ends with Section 5, where the main conclusions of our numerical investigation are presented.

2. DESCRIPTION OF THE GALACTIC MODEL

Our aim is to determine the interplay between ordered and chaotic motion of stars moving in the meridional plane of a time-dependent axially symmetric disk galaxy with a central spherically symmetric nucleus when the parameters of the model potential evolve in time. For this purpose, we use the usual cylindrical coordinates (R, ϕ, z), where z is the axis of symmetry.

The total gravitational potential $\Phi(R, z)$ consists of two components: the nucleus potential $\Phi_{\rm n}$ and the flat disk potential $\Phi_{\rm d}$. For the description of the spherically symmetric central nucleus, we use a Plummer potential (e.g., Binney & Tremaine 2008)

$$\Phi_{\rm n}(R, z) = \frac{-GM_{\rm n}}{\sqrt{R^2 + z^2 + c_{\rm n}^2}}. \tag{1}$$

Here G is the gravitational constant, while $M_{\rm n}$ and $c_{\rm n}$ are the mass and the scale length of the nucleus, respectively. This potential has been successfully used in the past to model and, therefore, interpret the effects of the central mass component in a galaxy (see e.g., Hasan & Norman 1990; Hasan et al. 1993; Zotos 2012; Zotos & Carpintero 2013; Zotos 2014a). At this point, it must be emphasized that we do not include any relativistic effects, because the nucleus represents a bulge rather than a black hole or any other compact object.

The galactic disk, on the other hand, is represented by the well-known Miyamoto-Nagai potential Miyamoto & Nagai (1975)

$$\Phi_{\rm d}(R, z) = \frac{-GM_{\rm d}}{\sqrt{R^2 + \left(\alpha + \sqrt{h^2 + z^2}\right)^2}}, \tag{2}$$

where, $M_{\rm d}$ is the mass of the disk, α is the scale length of the disk and h corresponds to the disk's scale height.

We use a system of galactic units where the unit of length is 1 kpc, the unit of velocity is 10 $\mathrm{km\,s^{-1}}$ and $G = 1$. Thus, the unit of mass is $2.325 \times 10^7 \mathrm{M}_\odot$, that

of time is 0.9778×10^8 yr, the unit of angular momentum (per unit mass) is 10 km kpc s^{-1}, and the unit of energy (per unit mass) is 100 $km^2 s^{-2}$. In these units, the values of the involved parameters are: $c_n = 0.25$, $\alpha = 3$, $h = 0.175$, while M_n and M_d are treated as variable parameters with time. The above-mentioned set of values of the parameters which are kept constant throughout the numerical calculations secures positive mass density everywhere and free of singularities.

For simplicity, we assume that mass is transported from the disk to the nucleus, in such as way, that we have a linear increase in the mass of the nuclear core, while a simultaneous linear decrease in the mass of the disk takes place. The linear mass transportation follows the equations

$$\begin{aligned} M_n &= M_{n0} + k\ t, \\ M_d &= M_{d0} - k\ t, \end{aligned} \tag{3}$$

where M_{n0} and M_{d0} are the initial values of the mass of the nucleus and the disk, respectively, while $k > 0$ is the proportionality constant which determines the timescale of the galactic evolution. We choose $M_{n0} = 0$, $M_{d0} = 7500$ and $k = 0.05$, so at the beginning of the galactic evolution ($t = 0$) there is no nucleus formed and all the mass is concentrated in the disk. We also assume that the linear rate described by Eqs. (3) is slow compared to the orbital period of the stars and is therefore adiabatic. This is true because the mass transportation lasts for 10^4 time units, while the orbital period is about two orders of magnitude smaller. Furthermore, the mass transportation and the galactic evolution stops after 10^4 time units when the final value of the mass of the nucleus and that of the disk is $M_n = 500$ and $M_d = 7000$, respectively. The particular final values of the parameters were chosen with a Milky Way-type galaxy in mind (e.g., Allen & Santillán 1991). It is well known, that such mass transportation mechanisms are usually met in the central regions of active galaxies and they are responsible for the enormous luminosity of the quasars which are hosted in the active galactic nuclei of the galaxies (see e.g., Collin & Zahn 1999). This is the main reason why we refer to the central mass concentration as a "nucleus" rather than as bulge (see also Zotos 2012).

The circular velocity in the galactic plane where $z = 0$ (see e.g., Zotos 2011) is undoubtedly one of the most important physical quantities in disk galaxies and can be calculated as

$$\theta(R) = \sqrt{R \left| \frac{\partial \Phi(R,z)}{\partial R} \right|_{z=0}}. \tag{4}$$

In Fig. 1 we present a plot of $\theta(R)$ at the beginning ($t = 0$) and at the end ($t = 10000$) of the galactic evolution. The red line corresponds to the case where $M_n = 0$ and $M_d = 7500$, that is when the central nucleus is absent, while the green line corresponds to the case where $M_n = 500$ and $M_d = 7000$ and a fully developed dense, massive nucleus lies in the galactic core. It is seen that at relatively low galactocentric distances ($R \leq 5$ kpc) the pattern of the two curves is completely different, while at large distances from the galactic center ($R > 5$ kpc), on the other hand, both curves fully coincide. We also observe the characteristic local minimum (at $R \simeq 1$ kpc) of the rotation curve when the massive nucleus is present, which appears when fitting observed data to a galactic model (e.g., Gómez et al. 2010; Irrgang et al. 2013).

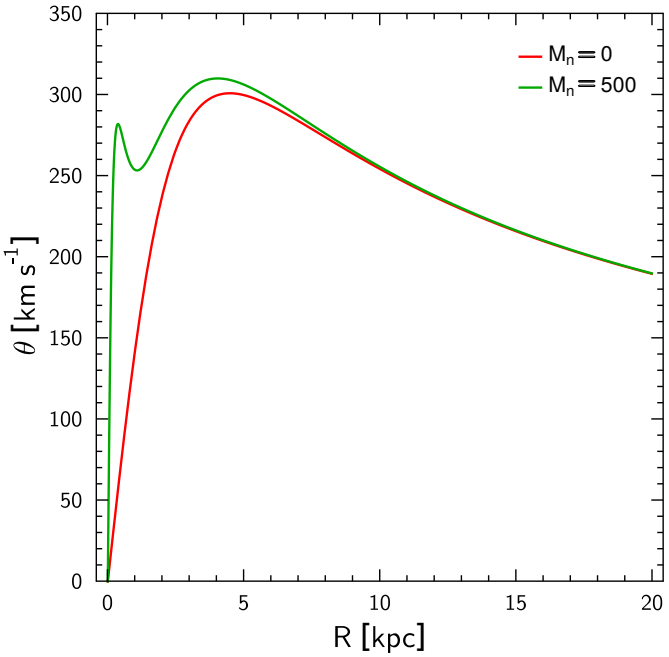

Fig. 1. A plot of the total circular velocity of our galactic model when $M_{\rm n} = 0$ and $M_{\rm d} = 7500$ (red) and when $M_{\rm n} = 500$ and $M_{\rm d} = 7000$ (green).

Exploiting the fact that the L_z-component of the total angular momentum is conserved because the gravitational potential $\Phi(R, z)$ is axially symmetric, orbits can be described by means of the effective potential

$$\Phi_{\rm eff}(R, z) = \Phi(R, z) + \frac{L_z^2}{2R^2}. \tag{5}$$

In this case, the basic equations of motion on the meridional plane take the form

$$\ddot{R} = -\frac{\partial \Phi_{\rm eff}}{\partial R}, \quad \ddot{z} = -\frac{\partial \Phi_{\rm eff}}{\partial z}, \tag{6}$$

while the equations governing the evolution of a deviation vector $\mathbf{w} = (\delta R, \delta z, \delta \dot{R}, \delta \dot{z})$, which joins the corresponding phase space points of two initially nearby orbits, needed for the calculation of the standard indicators of chaos (the SALI in our case), are given by the following variational equations

$$\begin{aligned}
(\dot{\delta R}) &= \delta \dot{R}, \quad (\dot{\delta z}) = \delta \dot{z}, \\
(\dot{\delta \dot{R}}) &= -\frac{\partial^2 \Phi_{\rm eff}}{\partial R^2} \delta R - \frac{\partial^2 \Phi_{\rm eff}}{\partial R \partial z} \delta z, \\
(\dot{\delta \dot{z}}) &= -\frac{\partial^2 \Phi_{\rm eff}}{\partial z \partial R} \delta R - \frac{\partial^2 \Phi_{\rm eff}}{\partial z^2} \delta z.
\end{aligned} \tag{7}$$

Consequently, the corresponding Hamiltonian to the effective potential given

in Eq. (5) can be written as

$$H = \frac{1}{2}\left(\dot{R}^2 + \dot{z}^2\right) + \Phi_{\rm eff}(R, z) = E, \tag{8}$$

where $\dot{R}$ and $\dot{z}$ are momenta per unit mass, conjugate to R and z, respectively, while E is the numerical value of the Hamiltonian, which is conserved only in the time-independent model. Therefore, an orbit is restricted to the area in the meridional plane satisfying $E \geq \Phi_{\rm eff}$, while all other regions are forbidden to the star.

3. COMPUTATIONAL METHODS

In order to examine the orbital dynamics (regularity or chaoticity) of the galaxy model, we need to establish some samples of initial conditions of orbits. The best approach, undoubtedly, would be to extract these samples of orbits from the distribution function of the model potential. Unfortunately, this is not available, so we followed another course of action. To determine the character of the orbits in our model, we chose dense grids of initial conditions in the phase $(R, \dot{R})$ space regularly distributed in the area allowed by the value of the value of the Hamiltonian E. At this point we have to point out that the value of the energy controls the grid size and particularly the $R_{\rm max}$ which is the maximum possible value of the R coordinate. On this basis, we chose as initial energy level the value $E_0 = -480$ which yields $R_{\rm max} \simeq 15$ kpc. Moreover, the angular momentum of all orbits is $L_{\rm z} = 10$ and remains constant throughout. Since the Hamiltonian of our model is time-dependent, its value is *not* conserved during the galactic evolution. To determine the change in the value of the Hamiltonian, i.e. $dE = (E - E_0)/E_0$, we chose 10000 random initial conditions in the phase space with $E_0 = -480$ and we recorded the value of the Hamiltonian of every orbit during the galactic evolution until $t = 10^4$ time units when the mass transportation stops. Our results are presented in Fig. 2 where we observe the evolution of the value of Hamiltonian as a function of time. It was found that for all integrated orbits their energy is linearly reduced with time within the gray-shaded area of the plot. Furthermore, the change of the value of the Hamiltonian ranges from about 3.5% to 4.8% and the black, dashed lines in Fig. 2 indicate the corresponding minimum and maximum linear trends.

Taking into account that the range of values regarding the change of the Hamiltonian is relatively small, we decided to adopt an average linear change for all orbits in our model. Our calculations show that the average Hamiltonian change, shown in blue in Fig. 2, follows the linear rule

$$E = E_0 - q\ t, \tag{9}$$

where $E_0 = -480$, while $q = 0.002$ so that $E = -500$ at $t = 10^4$ time units. Relation (9) is a powerful tool because it allows us to know the exact value of the Hamiltonian at every time step of the galactic evolution. Now we can use this valuable information in order to explore the orbital structure of the galaxy at various time points during the mass transportation. In particular, since we have equations describing the time-evolution of $M_{\rm n}$, $M_{\rm d}$ and E, we can pick some time points t_i, freeze the mass transportation and use the time-independent model in

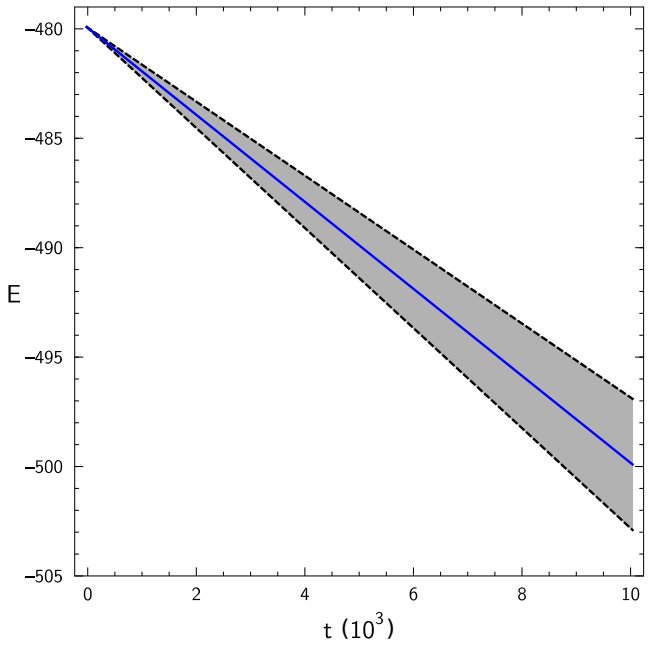

Fig. 2. Evolution of the value of the time-dependent Hamiltonian as a function of time for 10000 orbits initiated at the phase $(R, \dot{R})$ space with $E_0 = -480$. The blue line indicates the average Hamiltonian change, while the black, dashed lines delimit the boundaries of the energy variation dE.

order to integrate and classify the orbits, following the numerical approach used in Manos et al. (2013). Therefore, for each set of values of $M_{\rm n}(t_i)$ and $M_{\rm d}(t_i)$, we define a dense grid of initial conditions in the phase space regularly distributed in the area allowed by the corresponding value of the Hamiltonian $E(t_i)$. The step separation of the initial conditions along the R and $\dot{R}$ axes (or, in other words, the density of the grid) was controlled in such a way that always there are at least 50000 orbits to be integrated and classified. The grids of initial conditions of orbits whose properties will be examined are defined as follows: we consider orbits with initial conditions $(R_0, \dot{R}_0)$ with $z_0 = 0$, while the initial value of $\dot{z}_0$ is obtained from the Hamiltonian (8). For each initial condition, we numerically integrated the equations of motion (6) as well as the variational equations (7) with a double precision Bulirsch-Stoer `FORTRAN 77` algorithm (e.g., Press et al. 1992) with a small time step of the order of 10^{-2}, which is sufficient enough for the desired accuracy of our computations (i.e., our results practically do not change by halving the time step). In all cases, the energy integral[1] (Eq. 8) was conserved better than one part in 10^{-11}, although for most orbits it was better than one part in 10^{-12}.

For determining the regular or chaotic nature of orbits, we chose the SALI

[1]Remember that these orbits are integrated in the frozen time-independent model, where the energy integral is valid.

indicator Skokos (2001). The time-evolution of SALI strongly depends on the nature of the computed orbit since when an orbit is regular the SALI exhibits small fluctuations around non-zero values, while on the other hand, in the case of a chaotic orbit, the SALI after a small transient period tends exponentially to zero approaching the limit of the accuracy of the computer (10^{-16}). Therefore, the particular time-evolution of the SALI allow us to distinguish fast and safely between regular and chaotic motion. Nevertheless, we have to define a specific numerical threshold value for determining the transition from regularity to chaos. After conducting extensive numerical experiments, integrating many sets of orbits, we conclude that a safe threshold value for the SALI, taking into account the total integration time of 10^4 time units, is the value 10^{-7}. In order to decide whether an orbit is regular or chaotic, one may follow the usual method according to which we check, after a certain and predefined time interval of numerical integration, if the value of SALI has become less than the established threshold value. Therefore, if SALI $\leq 10^{-7}$ then the orbit is chaotic, while if SALI $> 10^{-7}$ then the orbit is regular. However, depending on the particular location of each orbit, this threshold value can be reached more or less quickly, as there are phenomena that can hold off the final classification of an orbit (i.e., there are special orbits called "sticky" orbits, which behave regularly for long time periods before they finally drift away from the boundaries of regular regions and start to wander in the chaotic domain, thus revealing their true chaotic nature fully. For the computation of SALI we used the `LP-VI` code Carpintero et al. (2014), a fully operational routine which efficiently computes a suite of many chaos indicators for dynamical systems in any number of dimensions.

Each orbit in the frozen time-independent Hamiltonian was numerically integrated for a time interval of 10^4 time units (10^{12} yr), which corresponds to a time span of the order of hundreds of orbital periods. The particular choice of the total integration time is an element of great importance, especially in the case of the sticky orbits. A sticky orbit could be easily misclassified as regular by any chaos indicator[2], if the total integration interval is too small, so that the orbit does not have enough time to reveal its true chaotic character. Thus, all the initial conditions of the orbits of a given grid were integrated, as we already said, for 10^4 time units, thus avoiding sticky orbits with a stickiness at least of the order of 10^2 Hubble times. All the sticky orbits that do not show any signs of chaoticity for 10^4 time units are counted as regular orbits since such vast sticky periods are completely out of the scope of our research.

A vital clarification regarding the nomenclature of the orbits should be made before closing this Section. All orbits of an axially symmetric potential are in fact three-dimensional (3D) loop orbits, i.e., orbits that always rotate around the axis of symmetry in the same direction. However, in dealing with the meridional plane, the rotational motion is lost, so the path that the orbit follows onto this plane can take any shape, depending on the nature of the orbit. Following the same approach of the previous papers of this series, we characterize an orbit according to its behavior in the meridional plane. If, for example, an orbit is a rosette lying in the equatorial plane of the axisymmetric potential, it will be a linear orbit in

[2] Generally, dynamical methods are broadly split into two types: (i) those based on the evolution of sets of deviation vectors to characterize an orbit and (ii) those based on the frequencies of the orbits that extract information about the nature of motion only through the basic orbital elements without the use of deviation vectors.

Table 1. Types and initial conditions of the orbits shown in Fig. 3(a-h). In all cases, $z_0 = 0$, $\dot{z}_0$ is found from the Hamiltonian, Eq. (8), while $T_{\rm per}$ is the period of the resonant parent periodic orbits.

Figure	Type	R_0	$\dot{R}_0$	$T_{\rm per}$
3a	box	1.20000000	0.00000000	-
3b	2:1 banana	6.94608753	0.00000000	1.82936813
3c	1:1 linear	3.48802471	38.08701776	1.52281338
3d	2:3 boxlet	14.12356085	0.00000000	3.07990781
3e	4:3 boxlet	12.62569659	0.00000000	5.95238344
3f	6:5 boxlet	13.27429077	0.00000000	9.51868683
3g	4:5 boxlet	14.30689514	0.00000000	6.47237905
3h	chaotic	0.12000000	0.00000000	-

the meridional plane, a tube orbit it will be a 2:1 orbit, etc. We should emphasize that we use the term "box orbit" for an orbit that conserves circulation, but this refers *only* to the circulation provided by the meridional plane itself. Because of the their boxlike shape in the meridional plane, such orbits were originally called "boxes" (e.g., Ollongren 1962), even though their three-dimensional shapes are more similar to doughnuts (more details can be found in the review of Merritt 1999). Nevertheless, we kept this formalism to maintain continuity with all the previous papers of this series.

4. NUMERICAL RESULTS

This Section contains the main numerical results of both the time-independent and the time-evolving model. In particular, we numerically integrate several sets of orbits, in an attempt to determine the regular or chaotic nature of motion of stars. First we begin with the time-independent model and use the sets of initial conditions described in the previous section to construct the respective grids, always adopting values inside the limiting curve. In all cases, the initial value of the energy was set equal to -480, while the angular momentum of the orbits is $L_{\rm z} = 10$. To study how the mass transportation from the disk to the central nucleus influences the level of chaos, we choose representative time points of the galactic evolution such as $t_i = \{0, 2000, 4000, ..., 10000\}$. Once the exact values of the parameters $M_{\rm n}$, $M_{\rm d}$ and E are known through Eqs. (3) and (9), we compute a set of initial conditions as described in Section 3 and we integrate the corresponding orbits computing the SALI of the orbits and then classifying regular orbits into different families.

Our numerical investigation suggests that in our galaxy model there are eight basic types of orbits: (i) chaotic orbits; (ii) box orbits; (iii) 1:1 linear orbits; (iv) 2:1 banana-type orbits; (v) 2:3 fish-type orbits; (vi) 4:3 resonant orbits; (vii) 6:5 resonant orbit and (viii) orbits with other secondary resonances (i.e., all resonant orbits not included in the former categories). It turns out that for each resonant family included in the "other category" the corresponding percentage is less than 1% in all cases, and therefore their contribution to the overall orbital structure of

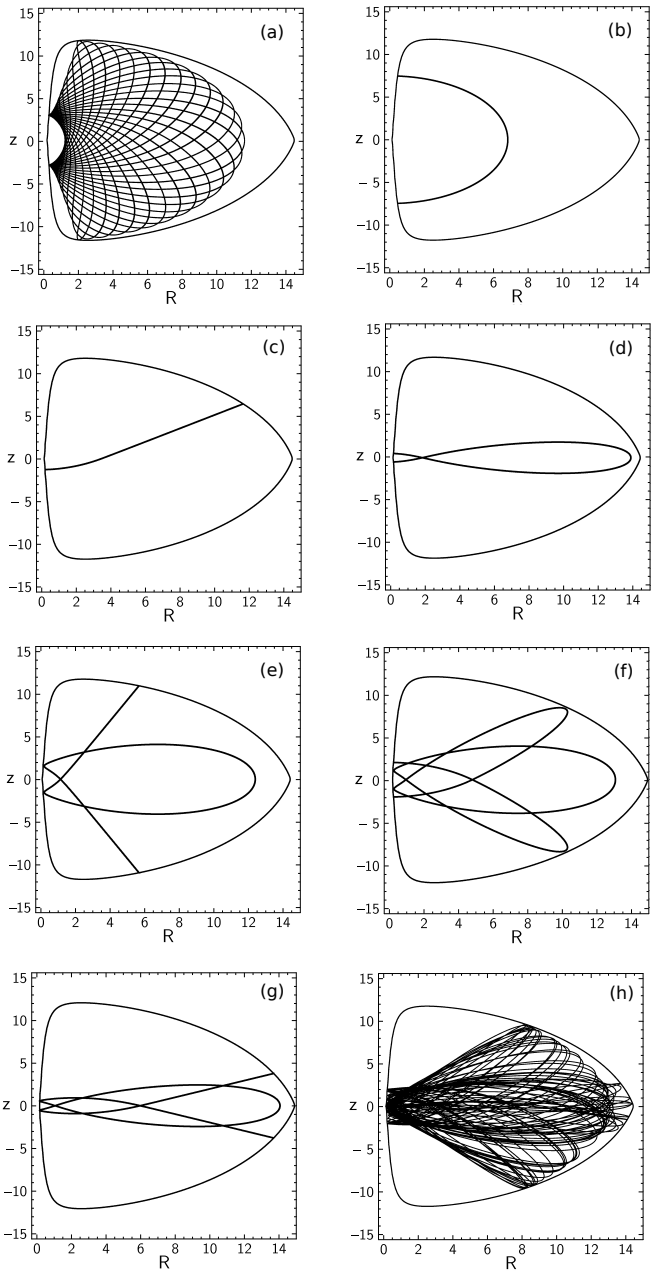

Fig. 3. Orbit collection of the basic types of orbits in our galaxy model: (a) box orbit; (b) 2:1 banana-type orbit; (c) 1:1 linear orbit; (d) 2:3 fish-type orbit; (e) 4:3 boxlet orbit; (f) 6:5 boxlet orbit; (g) 4:5 boxlet orbit, one of our "orbits with other resonance"; (h) chaotic orbit.

the galaxy is practically insignificant. The $n:m$ notation[3] we use for the regular orbits is according to Carpintero & Aguilar (1998) and Zotos & Carpintero (2013), where the ratio of those integers corresponds to the ratio of the main frequencies of the orbit, where main frequency is the frequency of greatest amplitude in each coordinate. Main amplitudes, when having a rational ratio, define the resonances of an orbit. In Fig. 3(a-h) we present examples of each of the basic types of regular orbits, plus an example of a chaotic one. In all cases, we set $M_{\rm n} = 500$ and $E = -500$ (except for the 4:5 and 6:5 resonant orbits, where $M_{\rm n} = 100$ and $E = -484$). The orbits shown in Figs. 3a and 3h were computed until $t = 100$ time units, while all the parent periodic orbits Zotos (2013) were computed until one period has completed. The outermost black curve circumscribing each orbit is the limiting Zero Velocity Curve (ZVC) in the meridional plane which is defined as $\Phi_{\rm eff}(R, z) = E$. Table 1 shows the types and the initial conditions for each of the depicted orbits; for the resonant cases, the initial conditions and the period $T_{\rm per}$ correspond to the parent[4] periodic orbits.

We would like to point out at this point, that the 1:1 resonance is usually the hallmark of the loop orbits and both coordinates oscillate with the same frequency in their main motion. Their mother orbit is a closed loop orbit. Moreover, when the oscillations are in phase, the 1:1 orbit degenerates into a linear orbit (the same as in Lissajous figures made with two oscillators). In our meridional plane, however, 1:1 orbits do not have the shape of a loop. In fact, their mother orbit is linear (e.g., Fig. 3c), and thus they do not have a hollow (in the meridional plane), but fill a region around the linear mother, always oscillating along the R and z directions with the same frequency. We designate these orbits "1:1 linear open orbits" to differentiate them from true meridional plane loop orbits, which have a hollow and also always rotate in the same direction.

In the following Figs. 4(a-f) we present six grids of initial conditions $(R_0, \dot{R}_0)$ of orbits that we have classified for different values of the final mass of the nucleus $M_{\rm n}$ in the frozen time-independent model. These color-coded grids of initial conditions are equivalent to the classical Poincaré Surfaces of Section (PSS) and allow us to determine what types of orbits occupy specific areas in the phase $(R, \dot{R})$ plane and also to follow the changes that orbits undergo. The outermost black thick curve is the limiting curve which is defined as

$$\frac{1}{2}\dot{R}^2 + \Phi_{\rm eff}(R, z = 0) = E. \tag{10}$$

In Fig. 4a which corresponds to time point $t = 0$ where the central nucleus is absent $(M_{\rm n} = 0)$ we observe that the entire phase plane is covered by initial conditions of regular orbits, while chaotic motion, if any, is negligible. In particular, initial conditions of box orbits occupy the vast majority of the phase space, a well-formed island of 2:1 resonant orbits is present at the center of the grid, while there are also several smaller stability islands of other resonant orbits embedded in the extended box area. The structure of the phase plane however, changes drastically

[3] A $n:m$ resonant orbit would be represented by m distinct islands of invariant curves in the $(R, \dot{R})$ phase plane and n distinct islands of invariant curves in the $(z, \dot{z})$ surface of section.

[4] For every orbital family there is a parent (or mother) periodic orbit, that is, an orbit that describes a closed figure. Perturbing the initial conditions which define the exact position of a periodic orbit we generate quasi-periodic orbits that belong to the same orbital family and librate around their closed parent periodic orbit.

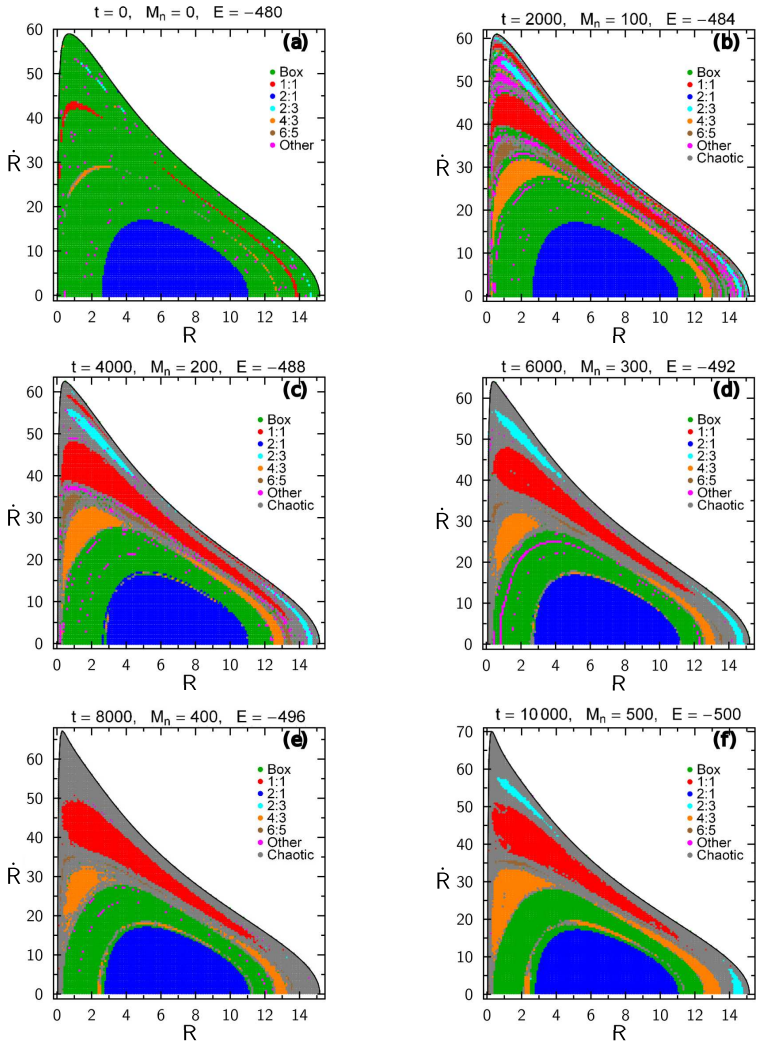

Fig. 4. Orbital structure of the phase $(R, \dot{R})$ plane of our galaxy model at several time points of the galactic evolution.

in Fig. 4b at $t = 2000$ time units when $M_{\rm n} = 100$. It is seen that the box area is significantly reduced and especially at the outer parts of the phase plane there is a strong presence of stability islands of resonant orbits surrounded by a thin chaotic layer. It is interesting to note that inside this chaotic layer one may identify several sets of tiny stability islands corresponding to higher resonant orbits which in our classification belong to the "other" category. The area on the phase plane occupied by these secondary higher resonant orbits is considerably confined when $t = 4000$ time units and $M_{\rm n} = 200$. Indeed we see in Fig. 4c that the corresponding stability islands are hardly visible, while at the same time the chaotic zone is amplified. The same pattern continues in Fig. 4d for $t = 6000$

time units and $M_{\rm n} = 300$ where the chaotic area is more prominent, while some thin filaments of initial conditions of secondary resonant inside the box region are observed. The mass transport is still in progress and for $t = 8000$ time units which corresponds to $M_{\rm n} = 400$ there is a major difference in the phase space, that is the absence of the 2:3 stability islands. Additional numerical calculations reveal that for $M_{\rm n} = 400$ the 2:3 resonance is unstable. This means that the periodic point of the 2:3 resonance is indeed present in Fig. 4e, although evidently deeply buried in the chaotic domain. Finally, in Fig. 4f, where $t = 10000$ time units and $M_{\rm n} = 500$, we observe that the 2:3 stability islands reappear in the phase space.

Looking carefully the color-coded grids presented in Figs.4(a-f) we can distinguish the location of the seven main types of regular orbits discussed earlier: (i) 2:1 banana-type orbits located to the central region of the grid; (ii) box orbits situated mainly outside of the 2:1 resonant orbits; (iii) 1:1 open linear orbits form the elongated island of initial conditions; (iv) 2:3 fish-type resonant orbits form the set of three small islands[5] at the outer parts of the grid; (v) 4:3 resonant orbits form the chain of three islands; (vi) 6:5 resonant orbits producing five small stability islands inside the chaotic region and (vii) other types of resonances producing extremely small islands embedded both in the chaotic and box areas. Chaos on the other hand, is mainly confined only at the outer parts of the phase plane. It is evident, that as the central nucleus becomes more and more massive gaining mass from the galactic disk, the amount of chaos in the phase space increases. It should also be mentioned that the allowed radial velocity $\dot{R}$ of the stars near the center of the galaxy is increasing during the galactic evolution, where the mass of the nucleus also increases.

The time-evolution of the percentages of the chaotic and all types of regular orbits as a function of the final mass of the central nucleus $M_{\rm n}$ is presented in Fig. 5. One may observe that at the beginning of the galactic evolution ($t = 0$) when the central nucleus is absent, there is no chaos whatsoever, and more than 70% of the phase space is dominated by initial conditions of box orbits. However, as mass begins to be transferred from the disk to the core, box orbits are depleted and this transportation starts to trigger chaotic motion. In particular, we see that as the nucleus becomes more and more massive with time the percentage of box orbits is significantly reduced and for $M_{\rm n} > 300$ it saturates around 25%, while at the same time the rate of chaotic orbits exhibits a considerable growth and for about $t > 6000$ time units chaotic orbits is the most populated family, although at high enough values of $M_{\rm n}$ their rate displays a minor decrease. At the end of the galactic evolution at $t = 10000$ time units, or in other words when $M_{\rm n} = 500$, the rates of box and chaotic orbits tend to a common value (around 25%), thus sharing half of the phase plane. Our numerical analysis suggests that the percentages of the rest of orbital families change very little during the galactic evolution. Indeed it is seen that the 2:1 resonant orbits (meridional bananas) are almost unperturbed by the shifting of the mass of the central nucleus occupying about 22% of the phase space throughout. Furthermore, the rates of the 1:1 and 4:3 resonant families display a monotone behavior roughly around 10% during the mass transportation. In addition, we may say that, in general terms, all the other resonant families (i.e.,

[5] It should be pointed out that the color-coded grids of Fig. 4(a-f) show only the $\dot{R} > 0$ part of the phase plane; the $\dot{R} < 0$ is symmetrical. Therefore, in many resonances not all the corresponding stability islands are present (e.g., for the 2:3 and 4:3 resonances only two (actually one and a half) of the three islands are shown).

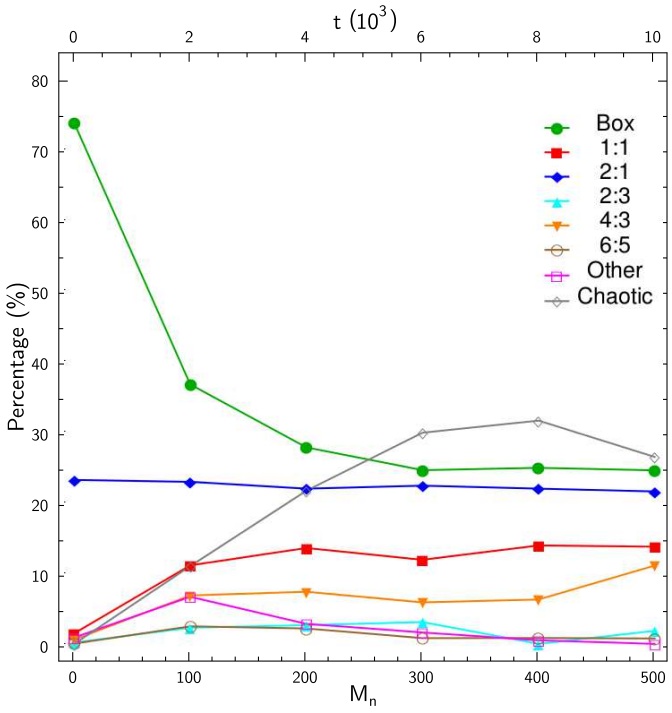

Fig. 5. Time-evolution of the percentages of the different types of orbits in the phase $(R, \dot{R})$ space of our galaxy model, as a function of the final mass of the nucleus $M_{\rm n}$.

the 2:3, 6:5 and "other") possess throughout very low percentages (always less than 5%) thus, the growth of the mass of the nucleus only shuffles the orbital content among them. Therefore, taking into account all the above-mentioned analysis, we may conclude that in the phase $(R, \dot{R})$ space the types of orbits that are mostly influenced by the mass transportation are the box and chaotic orbits. It is also interesting to note that the time-evolution of the percentages of the orbits is very similar to that given in Fig. 6 in Zotos & Carpintero (2013), where the influence of the mass of the nucleus in the time-independent version of same model was investigated.

All the previous numerical results correspond to specific time points off the galactic evolution. As it was explained in the previous Section, we can pick some characteristic time points, use the respective values of the mass of the disk, the mass of the nucleus and the value of the Hamiltonian and integrate orbits in the time-independent frozen model. Now we would like to investigate the character of orbits and the transition from regularity to chaos and vice versa during the mass transportation. For this purpose, we use the full time-dependent Hamiltonian as follows: we define in the phase space a grid of 50000 initial conditions of orbits with $E_0 = -480$ and we vary the mass of the nucleus form $M_{\rm n}(t_0 = 0) = 0$ to $M_{\rm n}(t_{\rm final} = 10000) = 500$ recording at each time step of the numerical integration the value of SALI. Our computations suggest that the nature of the orbits can change either from ordered to chaotic and vice versa or not change at all, as mass

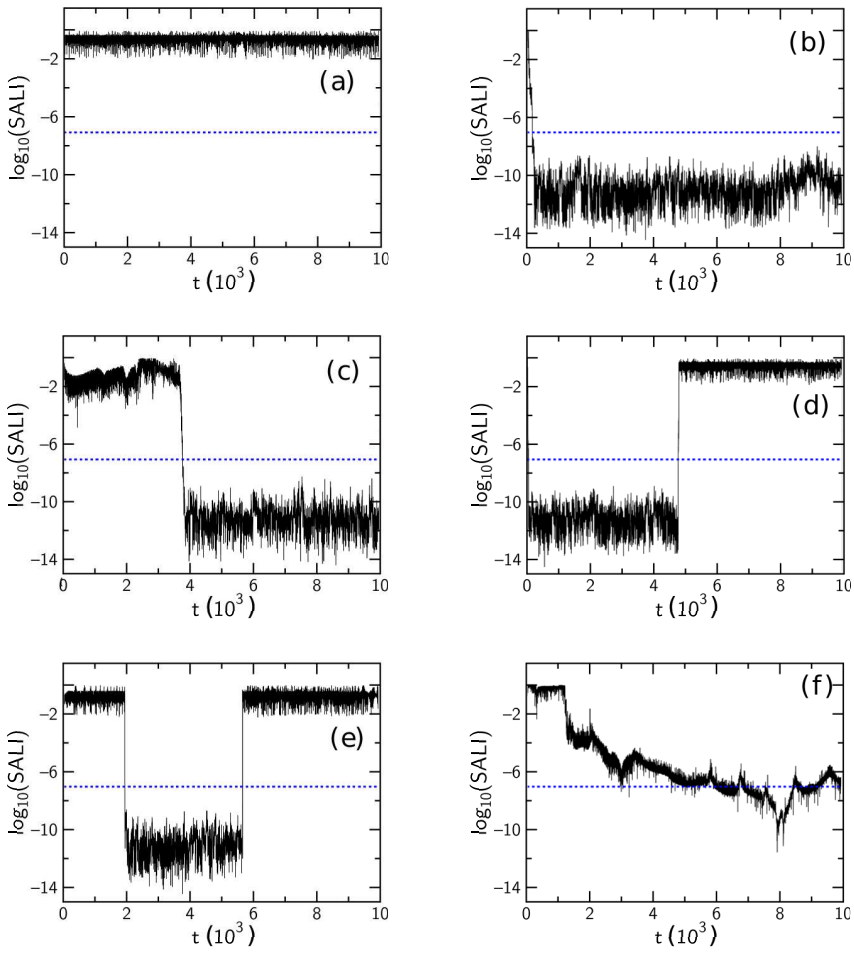

Fig. 6. Time-evolution of SALI for six different types of orbits in the time-dependent Hamiltonian. Details are given in the text.

is transported from the disk and a massive nucleus is developed in the central region of the galaxy. In Fig. 6(a-f) we present the time-evolution of SALI of six different orbits, as the total mass distribution of the galactic system changes with time, following the set of equations (3). For all six orbits we set $z_0 = 0$, $\dot{R}_0 = 0$, while $\dot{z}_0$ is obtained from the initial value of the Hamiltonian which is $E_0 = -480$. The horizontal, blue, dashed line in Fig. 6 corresponds to the threshold value (SALI $= 10^{-7}$) which separates regular from chaotic motion. Fig. 6a shows the time-evolution of SALI for an orbit with $R_0 = 7.5$. It is seen that the particular orbit starts as regular and remains regular throughout the galactic evolution. The pattern of SALI shown in Fig. 6b on the other hand, suggests that the orbit with $R_0 = 0.145$ maintains its chaotic character regardless the mass transportation. In Fig. 6c where $R_0 = 14.35$, we see that the orbit starts as regular but after about 3800 time units it becomes chaotic. The exact opposite scenario is shown in

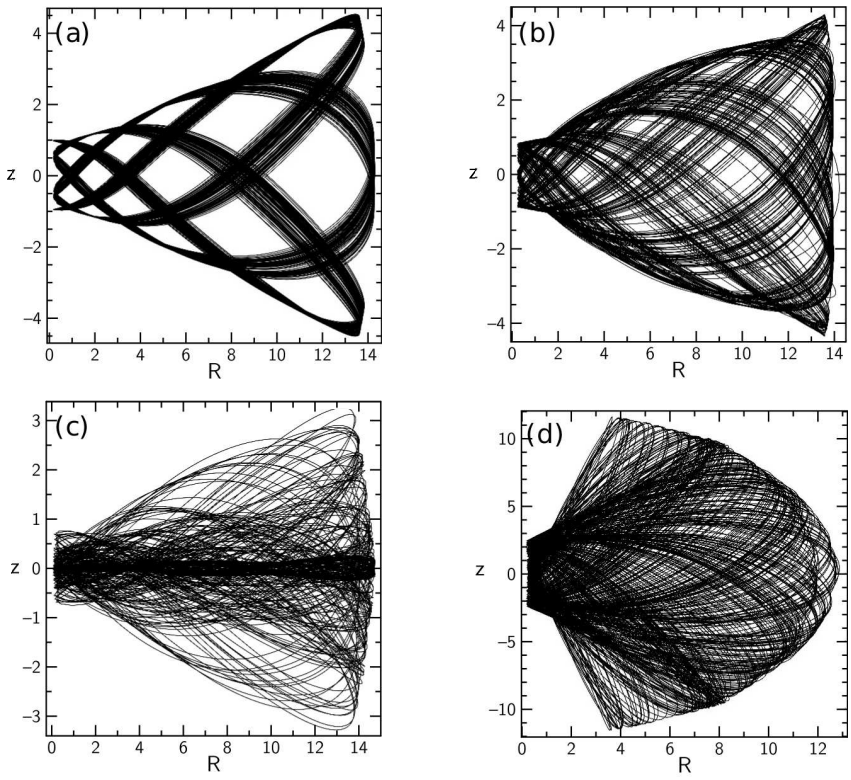

Fig. 7. The shape of the orbit discussed in Fig. 6c in four time intervals of the galactic evolution. (a-upper left): $0 \leq t \leq 500$; (b-upper right): $3500 \leq t < 3700$; (c-lower left): $3700 \leq t \leq 4100$; (d-lower right): $8000 \leq t \leq 8500$.

Fig. 6d where $R_0 = 0.23$. This orbit exhibits chaotic behavior for the first about 4800 time units of the galactic evolution however, for $t > 4800$ it clearly becomes regular. The transition from regularity to chaos and vice versa may occur more than one time during the mass transportation. Fig. 6e shows such a characteristic example of an orbit with $R_0 = 0.2217$ which display s chaotic nature only in the interval $1950 < t < 5670$. Nevertheless, the determination of the character of an orbit is not always very easy. This becomes evident by inspecting Fig. 6f where one may observe that the SALI of the orbit with $R_0 = 0.21$ oscillates around the threshold value, thus preventing us from having a clear and definitive view regarding the character of this orbit, which probably remains sticky throughout the galactic evolution. We must point out that these dynamical transitions are not related by no means to stickiness or ordinary diffusion phenomena that occur in time-independent systems.

In order to have a more enlightening picture about the transition from order to chaos during the mass transportation we provide in Fig. 7(a-d) the shape on the meridional (R, z) plane of the orbit explained in Fig. 6c for four time intervals of the galactic evolution. Fig. 7a shows the orbit for the first 500 time units, where it is clearly seen that the orbit is beyond any doubt a regular 6:7 resonant orbit. In

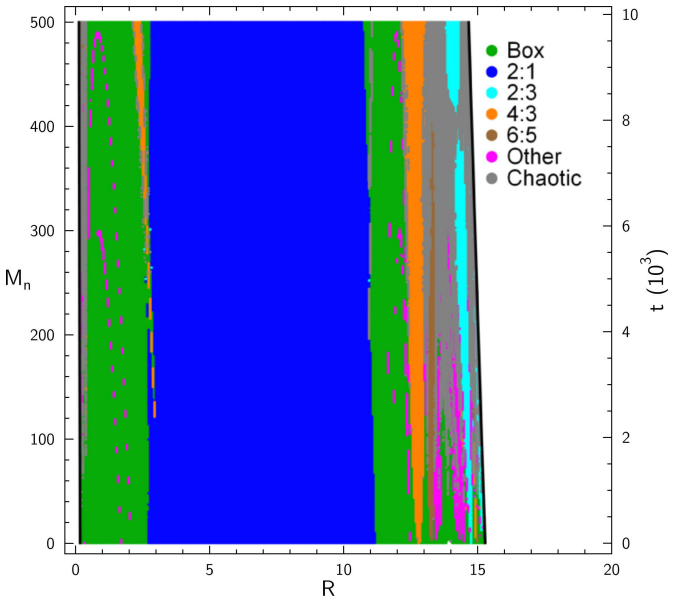

Fig. 8. Orbital structure of the $(R, M_{\rm n})$-plane. This diagram gives us a detailed analysis of the evolution of orbits starting perpendicularly to the R-axis when the mass of the nucleus varies in the interval $M_{\rm n} \in [0, 500]$ during the galactic evolution for $0 \leq t \leq 10000$ time units.

Fig. 7b where $3500 \leq t < 3700$ we observe that the path of the trajectory the star follows becomes very unclear which is an indication of imminent chaotic motion. Indeed in Fig. 7c where $3700 \leq t \leq 4100$ we see that the transition from regularity to chaos has been completed, according to the corresponding time-evolution of SALI which reported the transition point around 3800 time units. Moreover, it is observed in Fig. 7c that the test particle (star) spends a great deal of time moving very close to the galactic plane. Finally, in Fig. 7d where $8000 \leq t \leq 8500$, that is an advanced stage of the galactic evolution where the nucleus is massive enough, the complete chaotic nature of the orbits is fully revealed and the star moves at relatively high distances from the galactic plane up to about 10 kpc. It should be stressed out however, that the shape of an orbit gives only fast and qualitative information which sometimes can be inconclusive or even misleading regarding the nature of the orbit. Therefore, only highly accurate methods that use certain and objective numerical criteria, such as the SALI, should be used for determining the characters of orbits.

The color-coded grids of initial conditions in the phase $(R, \dot{R})$ plane presented in Fig. 4(a-f) provide information on the phase space mixing for only a specific time point of the galactic evolution and for the corresponding value of the mass of the nucleus $M_{\rm n}$. Following Hénon's idea Hénon (1969) however, we can consider a plane which provides information about regions of regularity and regions of chaos using the section $z = \dot{R} = 0$, $\dot{z} > 0$, i.e., the test particles (stars) are launched on the R-axis, parallel to the z-axis and in the positive z-direction. Thus, in contrast to the previously discussed grids (Fig. 4(a-f)), only orbits with pericenters on the R-axis are included and, therefore, the value of $M_{\rm n}$ is now used as an ordinate. In

this way, we can monitor how the mass of the nucleus influences the overall orbital structure of our dynamical system using a continuous spectrum of values of $M_{\rm n}$ rather than a few discrete ones. Fig. refRt shows the orbital structure of the $(R, M_{\rm n})$-plane, when $M_{\rm n} \in [0, 500]$ and $0 \leq t \leq 10000$ time units. In order to be able to monitor with sufficient accuracy and details the evolution of the families of orbits, we defined a dense grid of 10^5 initial conditions in the $(R, M_{\rm n})$-plane. For creating this plane we use the time-independent model with the values of $M_{\rm n}$, $M_{\rm d}$ and E according to Eqs. (3) and (9). It is evident, that the vast majority of the grid is covered either by box or 2:1 resonant orbits, while initial conditions of chaotic orbits are mainly situated to right outer part of the $(R, M_{\rm n})$-plane. Furthermore, the 2:3, 4:3 and 6:5 resonances produce thin vertical stability layers. Furthermore, our numerical calculations indicate that in the interval $396 \leq M_{\rm n} \leq 407$ there is no indication of the 2:3 resonance. This justifies why the stability islands of this resonance were found absent in Fig. 4e when $M_{\rm n} = 400$. It is also observed, that several families of higher resonant orbits are present, corresponding to thin filaments of initial conditions living inside the box region. We would like to note, that the maximum value of the R coordinate ($R_{\rm max}$) is slightly reduced as the nucleus gains mass. We must also point out that the $(R, M_{\rm n})$-plane contains only such orbits starting perpendicularly to the R-axis, while all types of orbits whose initial conditions are pairs of position-velocity (i.e., the 1:1 resonant family) are obviously not included.

5. CONCLUDING REMARKS

In the present work we have sought to shed some light on the interesting phenomenon of mass transportation by investigating the orbital dynamics of a mean filed galaxy model, when the mass parameters are linearly changing in time. For this purpose, we used an analytic, axially symmetric, time-dependent galactic gravitational model which embraces the general features of a disk galaxy with a dense, massive, central nucleus. During the galactic evolution the total mass of the galaxy remains constant which means that whatever mass the disk loses, it is gained by the nucleus. In order to simplify our numerical calculations we chose to work in the meridional (R, z) plane, thus reducing three-dimensional to two-dimensional motion. We kept the values of all the other parameters constant, because our main objective was to determine the influence of the mass of the nucleus on the percentages of the orbits, where mass is transported from the disk to the nucleus. Our thorough and detailed numerical analysis suggests that the level of chaos, as well as the different regular families, are indeed very dependent on the galactic evolution. Furthermore, we wanted to prove that transitions from regularity to chaoticity and vice versa are possible in this simple model.

Since a distribution function of the model potential was not available so as to use it for extracting different samples of orbits, we had to follow an alternative path. We defined for several time points of the galactic evolution, dense grids of initial conditions $(R_0, \dot{R}_0)$ regularly distributed in the area allowed by the corresponding value of energy on the phase space. To show how the mass transportation influences the orbital structure of the system, we presented for each case the color-coded grids of initial conditions, which allow us to visualize what types of orbits occupy specific areas in the phase space. Each orbit was numerically integrated in the time-independent Hamiltonian for a time period of 10^4 time units (10^{12}

yr), which corresponds to a time span of the order of hundreds of orbital periods. The particular choice of the total integration time was made in order to eliminate sticky orbits (classifying them correctly as chaotic orbits) with a stickiness at least of 100 Hubble times. Then, we made a step further in an attempt to distribute all regular orbits into different families. Therefore, once an orbit has been characterized as regular applying the SALI method, we then further classified it using a frequency analysis method. For the numerical integration of the grids with the initial conditions of the orbits, we needed about between 5 and 7 days of CPU time on a Pentium Dual-Core 2.2 GHz PC, depending on the rate of regular orbits in each case.

The most important outcomes of our numerical investigation can be summarized as follows:

• Numerous types of ordered orbits were identified in our disk galaxy model, while there are also extended chaotic domains separating the areas of regular motion. In particular, a plethora of resonant orbits (i.e., 1:1, 2:1, 2:3, 4:3, 6:5 and other resonant orbits) are present, thereby enriching the orbital structure of the galaxy. It should be clarified that by the term "other resonant orbits" we refer to resonant orbits with a rational quotient of frequencies made from integers > 5, which of course do not belong to the main families.

• It was observed that the galactic evolution, where mass is linearly transported from the disk to the central nucleus, influences mainly the percentages of box and chaotic orbits in the phase $(R, \dot{R})$ space. The mass of the central nucleus, although spherically symmetrical and therefore maintaining the axial symmetry of the entire galaxy, can generate substantial chaotic phenomena in the meridional plane, as it is above zero.

• We found that as the galactic nucleus becomes more and more massive the percentage of chaotic motion grows mainly at the expense of box orbits, while chaotic orbits is the dominant family once the mass of the nucleus has reached about 7% of the mass of the galactic disk. At early stages of the mass transportation, where the mass of the nucleus is still relatively low, we measured the largest amount of ordered orbits. In fact, when $M_{\rm n} < 100$ more than half of the phase space is covered by initial conditions of box orbits.

• Our results strongly indicate that in the time-dependent Hamiltonian system, where a massive nucleus is developed in the central region of the disk galaxy through the mass transportation, the character of the orbits can change either from ordered to chaotic and vice versa or not change at all.

• The SALI method was proved highly efficient and accurate in the identification of chaos in the time-dependent system. Our computations revealed that this indicator is especially suited for detecting time intervals where an orbit exhibits a fundamental change in its character. Specifically, by following the time-evolution of SALI one can determine in detail the orbit's successive transitions from regularity to chaoticity and vice versa.

Judging by the interesting findings we may say that our task has been successfully completed. We hope that the present numerical analysis and the corresponding results will be useful in the field of time-dependent galactic Hamiltonian systems. This is a promising step in the task of understanding the galactic evolution of disk galaxies with spherical nuclei. Taking into account that our results are encouraging, we are planning to properly modify our galactic model in order to expand our investigation into three dimensions and explore the entire

six-dimensional phase space. In addition, N-body simulations may elaborate the mass transportation and its implication on the evolution of galaxies.

ACKNOWLEDGMENTS. The author would like to express his warmest thanks to the anonymous referee for the careful reading of the manuscript and for all the apt suggestions and comments which allowed us to improve both the quality and the clarity of the paper.

REFERENCES

Allen C., Santillán A. 1991, RevMexAA, 22, 255
Binney J., Spergel D. 1982, ApJ, 252, 308
Binney J., Spergel D. 1984, MNRAS, 206, 159
Binney J. Tremaine S. 2008, Galactic Dynamics, Princeton Univ. Press, Princeton, USA
Caranicolas N.D., Papadopoulos N.J. 2003, A&A, 399, 957
Caranicolas N.D., Zotos E.E. 2013, PASA, 30, 49
Carpintero D.D., Aguilar L.A. 1998, MNRAS, 298, 1
Carpintero D.D., Maffione N., Darriba L. 2014, Astronomy and Computing, 5, 19
Collin S., Zahn J.P. 1999, A&A 344, 449
Gómez F., Helmi A., Brown A.G.A., Li Y.S. 2010, MNRAS, 408, 935
Hasan H., Norman C.A. 1990, ApJ, 361, 69
Hasan H., Pfenniger D., Norman C.A. 1993, ApJ, 409, 91
Hénon M. 1969, A&A, 1, 223
Irrgang A., Wilcox B., Tucker E., Schiefelbein L. 2013, A&A, 549, A137
Manos T., Bountis T., Skokos, Ch. 2013, Journal of Physics A, 46, 254017
Manos T., Machado, R.E.G. 2014, MNRAS, 438, 2201
Merritt D. 1999, PASP, 111, 129
Miyamoto W., Nagai R. 1975, PASJ, 27, 533
Muzzio J.C., Carpintero D.D., Wachlin F.C. 2005, CeMDA, 91, 173
Ollongren A. 1962, Bulletin of the Astronomical Institutes of the Netherlands, 16, 241
Papadopoulos N.J., Caranicolas N.D. 2006, Baltic Astronomy, 15, 561
Press H.P., Teukolsky S.A, Vetterling W.T., Flannery B.P. 1992, Numerical Recipes in FORTRAN 77, 2nd Ed., Cambridge Univ. Press, Cambridge, USA
Šidlichovský M., Nesvorný D. 1996, CeMDA, 65, 137
Skokos C. 2001, J. Phys. A Math. Gen., 34, 10029
Zotos E.E. 2011, New Astronomy, 16, 391
Zotos E.E. 2012, New Astronomy, 17, 576
Zotos E.E. 2013, Nonlinear Dynamics, 73, 931
Zotos E.E. 2014a, A&A, 563, A19
Zotos E.E. 2014b, Baltic Astronomy, 23, 37
Zotos E.E., Carpintero D.D. 2013, CeMDA, 116, 417
Zotos E.E., Caranicolas N.D. 2013, A&A, 560, A110
Zotos E.E., Caranicolas N.D. 2014, Nonlinear Dynamics, 76, 323